Inorganic Chemistry

Article

pubs.acs.org/IC

Enhanced Kinetic Stability of Pure and Y-Doped Tetragonal ZrO_2

Michaela Kogler,[†,⊥] Eva-Maria Köck,[†,⊥] Stefan Vanicek,[‡] Daniela Schmidmair,[§] Thomas Götsch,[†] Michael Stöger-Pollach,[∥] Clivia Hejny,[§] Bernhard Klötzer,[†] and Simon Penner*[,†]

[†]Institute of Physical Chemistry, [‡]Institute of Inorganic and Theoretical Chemistry, and [§]Institute of Mineralogy and Petrography, University of Innsbruck, A-6020 Innsbruck, Austria

[∥]University Service Center for Transmission Electron Microscopy (USTEM), Vienna University of Technology, Wiedner Hauptstrasse 120, A-1040 Vienna, Austria

Supporting Information

ABSTRACT: The kinetic stability of pure and yttrium-doped tetragonal zirconia (ZrO_2) polymorphs prepared via a pathway involving decomposition of pure zirconium and zirconium + yttrium isopropoxide is reported. Following this preparation routine, high surface area, pure, and structurally stable polymorphic modifications of pure and Y-doped tetragonal zirconia are obtained in a fast and reproducible way. Combined analytical high-resolution in situ transmission electron microscopy, high-temperature X-ray diffraction, and chemical and thermogravimetric analyses reveals that the thermal stability of the pure tetragonal ZrO_2 structure is very much dominated by kinetic effects. Tetragonal ZrO_2 crystallizes at 400 °C from an amorphous ZrO_2 precursor state and persists in the further substantial transformation into the thermodynamically more stable monoclinic modification at higher temperatures at fast heating rates. Lower heating rates favor the formation of an increasing amount of monoclinic phase in the product mixture, especially in the temperature region near 600 °C and during/after recooling. If the heat treatment is restricted to 400 °C even under moist conditions, the tetragonal phase is permanently stable, regardless of the heating or cooling rate and, as such, can be used as pure catalyst support. In contrast, the corresponding Y-doped tetragonal ZrO_2 phase retains its structure independent of the heating or cooling rate or reaction environment. Pure tetragonal ZrO_2 can now be obtained in a structurally stable form, allowing its structural, chemical, or catalytic characterization without in-parallel triggering of unwanted phase transformations, at least if the annealing or reaction temperature is restricted to $T \leq 400$ °C.

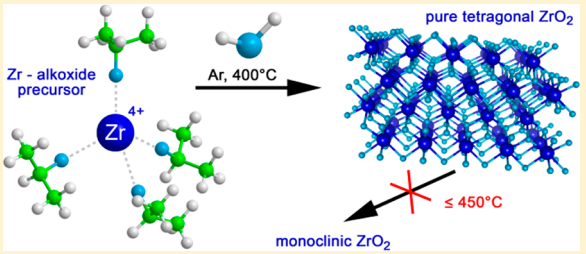

1. INTRODUCTION

Zirconia-containing materials have been and still are some of the most extensively studied oxide systems due to their outstanding material and physicochemical properties.[1−6] The application range encompasses disparate diametral research areas such as ceramics technology[2] or catalysis,[4] further confirming its outstanding technological role. Although recent interest lies more on its exploitation as functional material, zirconia-containing materials also represent one of the best-studied systems from a fundamental physicochemical point of view. This is mainly due to its polymorphic forms, which include monoclinic, tetragonal, cubic, and amorphous structures, the stabilities of which are reported to depend on particle size, gas phase pressure, temperature, or doping level.[5,7−9] Especially well-studied in this respect are the phase transformations between the different structures. The transformation between the tetragonal and the monoclinic phase is particularly well-understood on the atomic level and is assigned to a martensitic-type phase transformation, a diffusionless and athermic structural rearrangement involving cooperative shear movements of the structural entities.[5,10] However, apart from the fundamental scientific level, the interest in a better understanding for more application-oriented research is mainly fueled by the different structural, electronic, and (surface) chemical properties, giving rise to altered adsorption, catalytic, or general materials behavior. These differences are best seen in a comparison between undoped monoclinic ZrO_2 and Y-doped tetragonal ZrO_2, on one hand, and pure monoclinic and pure tetragonal ZrO_2, on the other hand. As for the former, Y stabilizes the tetragonal/cubic ZrO_2 structure. Y-stabilized ZrO_2 (YSZ) is used as an ionic conductor at high temperatures in solid-oxide fuel cells—in contrast to monoclinic ZrO_2.[11] Comparing the respective tetragonal and monoclinic ZrO_2 structures with respect to surface and adsorption chemistry, clear differences in the adsorption behavior arise, which, in due course, may eventually give rise to altered catalytic or materials behavior.[12−14] However, this discussion reveals an inherent drawback in the comparative characterization of such polymorphic forms: differences with respect to kinetic stability might trigger unwanted phase transformations during characterization of the phase under question and in consequence might lead to uncontrollable compositions of structural mixtures of, for example, monoclinic

Received: October 30, 2014
Published: December 4, 2014

   dx.doi.org/10.1021/ic502623t | Inorg. Chem. 2014, 53, 13247−13257

and tetragonal ZrO_2, while performing, for example, a catalytic reaction.[15−31] This might in turn obscure the unequivocal assignment of, for example, catalytic properties to the surface of a single-phase ZrO_2 support. Having said that, a number of different procedures exist to induce the formation of the room-temperature metastable tetragonal ZrO_2 polymorph, either via dedicated chemical preparation routines, for example, following an alkoxide decomposition pathway[7,15,16,18−21] or via structural stabilization exploiting particle size and crystallographic effects.[5,8,25,32] As for the latter, it has been determined theoretically and experimentally that the tetragonal structure is stable between grain sizes of 5 and 40 nm or that structural similarities between hydrous precursor species and the tetragonal ZrO_2 structure might aid the stabilization.[5,8,33,34] However, despite these efforts in preparation, the subsequent structural stability test and persistence against phase transformation under reaction conditions has, so far, not been focused upon in detail. For example, some adsorption studies using small test molecules like CO or CO_2 have been conducted at temperatures where other authors already observed a phase transformation.[15,16,18,19,21,27,28] In some cases, where the initial tetragonal ZrO_2 sample was clearly phase-pure after preparation, this purity was not reported after use.[12−14] Especially the presence of water in the gas phase was reported to induce the phase transformation, which might impose great disadvantages when using tetragonal ZrO_2 as a support in reforming processes.[35]

To close this knowledge gap, and to clarify the thermochemical stability issue, we herein report a detailed study of the preparation of structurally stable, clean, and pure as well as Y-doped tetragonal ZrO_2 materials starting from zirconium and yttrium isopropoxide precursors. The eventual phase transformations from the amorphous precursor to the tetragonal phase as well as to the monoclinic polymorph were studied structurally and kinetically using an array of in situ structure-determining methods (high-temperature, high-resolution transmission electron microscopy, high-temperature temperature-programmed X-ray diffraction). For complementary information on the chemical state during the transformations, X-ray fluorescence spectroscopy and thermogravimetric analysis coupled with differential scanning calorimetry and mass spectrometry were used. Additional morphological and structural information was obtained by ex situ scanning electron microscopy and Raman spectroscopy.

The effort of our work yielded not only a structurally stable, pure, and Y-stabilized high-surface area tetragonal ZrO_2 material but also detailed information on the kinetic limitations of the tetragonal-to-monoclinic phase transformation, which could, to some extent, be steered by carefully adjusting the experimental parameters. Subsequently, our approach, most importantly, offers the novel possibility to reliably characterize structural and catalytic properties of a pure, structurally stable tetragonal ZrO_2 sample in comparison to the Y-doped tetragonal ZrO_2 phase.

2. EXPERIMENTAL SECTION

2.1. Material Preparation. For preparing pure tetragonal zirconia and 8 mol % yttria-stabilized tetragonal zirconia, zirconium(IV) isopropoxide (isopropanol adduct, 99.9% Zr, Strem Chemicals) and yttrium(III) isopropoxide (isopropanol adduct, Strem Chemicals) were used as starting materials. The followed preparation routine is a variant of the one reported by Mazdiyasni et al. via decomposition of zirconium alkoxides and the subsequent hydrolysis of zirconium hydroxy aerogels.[15] This method is a fairly common preparation pathway to nanocrystalline zirconia polymorphs. Since our modified method is of paramount importance for preparation of different zirconia structures, we provide a concise discussion with respect to literature-reported data at the beginning of the Results and Discussion Sections.

The starting materials were weighed in a glovebox with a N_2 protective atmosphere being established during the whole preparation until final quenching with water. All used glass devices were baked at 100 °C to ensure completely water-free conditions. To obtain ∼4 g of final zirconia product, for pure tetragonal ZrO_2 12.58 g of zirconium(IV) isopropoxide, and, for 8 mol % yttria-stabilized tetragonal ZrO_2, 11.58 g of zirconium(IV) isopropoxide together with 0.64 g of yttrium(III) isopropoxide were dissolved in 260 mL of isopropanol (Finne Gatt-Koller, 99.98%). Isopropanol was added dropwise, and the suspension/solution was vigorously stirred during addition. In summary, 1 h and careful heating with a warm water bath (50 °C) were necessary to totally dissolve the isopropoxide materials. After recooling the solution to room temperature, a stoichiometric amount of 3.4 mL of water was then added dropwise. The resulting gel was stirred for an additional 30 min, and the solvent was removed on a rotary evaporator. The white powdery product was dried in vacuo at a constant temperature of 100 °C. In due course, the obtained aerogels were used as starting materials for all characterization experiments. Brunauer−Emmett−Teller (BET) measurements revealed specific surface areas of ZrO_2 of 12 $m^2\ g^{-1}$ after calcination at 400 °C, decreasing to 4 $m^2\ g^{-1}$ after calcination to 1000 °C. For YSZ, 21 $m^2\ g^{-1}$ was measured after calcination at 400 °C, decreasing to 8 $m^2\ g^{-1}$ at 1000 °C. Chemical analysis of all samples was performed using a Spectro XEPOS energy dispersive X-ray fluorescence analyzer (EDXRFA) and revealed purities of 99.99%. A representative analysis, including correlation to a commercially available monoclinic ZrO_2 compound, is provided in Table S1 in the Supporting Information.

2.2. X-ray Diffraction. High-temperature XRD data were collected with a Siemens D5005 diffractometer using $\theta-\theta$ coupling, parallel beam optics, and a scintillation counter using Cu $K_{\alpha1}$ and $K_{\alpha2}$ radiation. Scans were taken in the 2θ range from 10 to 70° with 0.02° 2θ steps and a counting time of 2 s $step^{-1}$. For high-temperature experiments the diffractometer is equipped with an Anton Paar HTK1200 temperature chamber.

Samples were prepared in a corundum sample holder. For the experiments with slower heating rate, scans measured in air were taken every 50 °C in the temperature range from 50 to 1000 °C. A heating rate of 0.1 °C s^{-1} between the particular temperature steps was applied. Taking into account that measuring a whole scan requires ∼105 min including an equilibration period of 5 min before every scan and a heating time of 8 min between the scans, the actual heating rate over the entire experiment is accordingly lower than 0.01 °C s^{-1}. The resulting length of the experiments varies between 1946 min (32 h 26 min; 400 °C), 2398 min (40 h; 600 °C), 2850 min (47 h 30 min; 800 °C), and 3302 min (55 h 2 min; 1000 °C).

For faster XRD measurements, the samples were annealed at 0.5 °C s^{-1} to the respective temperatures (600, 800, or 1000 °C), followed by an extended isothermal annealing period and recooling to room temperature also at 0.5 °C s^{-1} (all in air). The respective heating (or recooling) times are ∼19 min (600 °C), ∼26 min (800 °C), and ∼33 min (1000 °C). Immediately after reaching the required temperatures, the first scan was started. The time taken per scan was 100 min; 14 scans were taken at the respective highest temperatures, and additionally one was taken after recooling. The resulting length of the experiments varies between 1538 min (25 h 38 min; 600 °C), 1550 min (25 h 50 min; 800 °C), and 1565 min (26 h 05 min; 1000 °C).

For the measurements of the samples treated under moist conditions, a D8 Discover diffractometer in Bragg−Brentano geometry was used. The diffractometer is equipped with a Cu tube, a primary Ge monochromator, and a LYNXEYE detector. During the measurements, the samples were supported on a rotating Si single-crystal holder with suppressed background intensity. Scans were taken in the 2θ range from 10 to 70° with 0.01° 2θ steps and a counting time of 2 s $step^{-1}$.

dx.doi.org/10.1021/ic502623t | Inorg. Chem. 2014, 53, 13247−13257

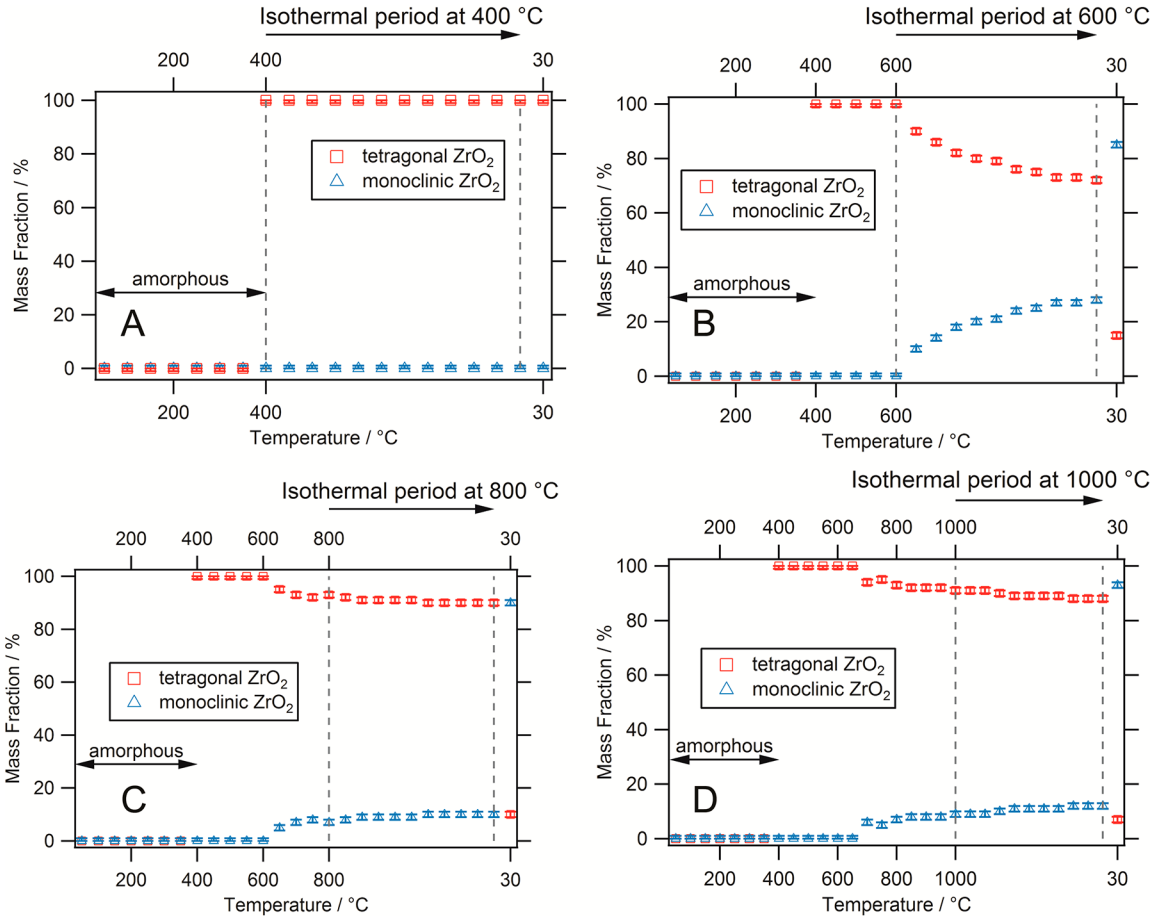

Figure 1. Representation of the high-temperature X-ray diffraction experiments on the pure ZrO_2 sample after different annealing treatments up to 400 °C (A), 600 °C (B), 800 °C (C), and 1000 °C (D). The colors of the markers denote the different tetragonal and monoclinic ZrO_2 phases. Dashed vertical lines denote the range of the isothermal periods (20 h for the experiment at 400 °C, 18 h 20 min for the experiments at 600, 800, and 1000 °C). The arrows indicate the presence range of amorphous ZrO_2.

For qualitative phase analysis, the software DIFFRAC^{plus} EVA[36] in combination with the database PDF-4+[37] was used. Phase quantification was performed with the software TOPAS[38] by employing the Rietveld method. Initial starting values for the structure refinements were taken from literature data.[39−41] In the course of the Rietveld refinement, scale factors, lattice parameters, and "size-like" Lorentzian and "strain-like" Gaussian peak broadening of the contributing phases were adjusted.

2.3. Transmission and Scanning Electron Microscopy. The samples were analyzed using a 200 kV FEI Tecnai F20 (scanning) transmission electron microscope ((S)TEM). The phases were identified by selected area electron diffraction (SAED) and high-resolution TEM (HRTEM). For the annealing treatments, a double tilt heating holder capable of operating at temperatures up to 1000 °C in vacuo was used.

All SEM experiments were conducted using an SM 982 GEMINI ZEISS Field Emission Scanning Electron Microscope. Prior to SEM imaging, the samples were coated with Au/Pd (10 nm) to improve conductance and were fixed with conducting carbon paste.

2.4. Thermogravimetric Analysis. The differential thermal analysis (DTA) experiment was performed on a Setaram SetsysEvolution 2400 instrument, using a TGA-DTA1600 transducer, equipped with Pt/Pt−Rh S-type thermocouples. The instrument is coupled with an OmniStar QMS200, Pfeifer Vacuum quadrupole mass spectrometer. For the first experiment, 19.80 mg of the pulverized ZrO_2 sample material was filled in a 100 μL Al_2O_3 crucible. Subsequently, after a routine prerun including evacuation and flooding the sample chamber with He, the DTA experiment was carried out by heating with a rate of 0.25 °C min^{-1} to a maximum temperature of 600 °C in He atmosphere and simultaneous recording of selected masses (m/z = 12, 15, 16, 17, 18, 28, 32, 44, 58, 59, 60, corresponding to carbonaceous fragments from the decomposition of the alkyl group, water, oxygen, CO, CO_2, and OH fragments). To avoid loss of material during application of vacuum to the samples, in a second experiment the prerun did not include vacuum but a thoroughly extended He flooding of the sample chamber. In this experiment, 10.46 mg of powder material was heated in a corundum crucible with a lid to 600 °C with 1 °C min^{-1} heating rate and kept at this temperature for the subsequent 5 h before finally cooling.

2.5. Raman Spectroscopy. Confocal Raman spectra of the polycrystalline samples in the range of 50−3800 cm^{-1} were recorded with a Horiba Jobin Yvon Labram-HR 800 Raman micro spectrometer. The samples were excited using the 532 nm (2.33 eV) emission line of a frequency-doubled 25 mW Nd:YAG laser under an Olympus 100× objective lens with a numerical aperture of 0.9. The size of the laser spot on the surface was approximately 1 μm in diameter. The scattered light was dispersed by an optical grating with 1800 lines mm^{-1} and collected by a 1024 × 256 open-electrode CCD detector. The spectral resolution, determined by measuring the Rayleigh line, was better than 2 cm^{-1}. The spectra were recorded in unpolarized mode at ambient conditions. The accuracy of the Raman line shifts, calibrated by measuring a silicon standard, was on the order of 0.5 cm^{-1}.

3. RESULTS

3.1. High-Temperature X-ray Diffraction. Structural analysis of the samples during preparation and eventual phase

dx.doi.org/10.1021/ic502623t | Inorg. Chem. 2014, 53, 13247−13257

transformation was mainly based on high-temperature X-ray diffraction and in situ electron microscopy (Section 3.2). Figure 1A–D shows experiments where the initially amorphous ZrO_2 gel precursor was heated to different temperatures with subsequent prolonged isothermal periods at the highest temperatures, before final cooling. Most notably, the average heating rate in these experiments is very slow, as outlined in detail in Section 2.2. in the Experimental Section. The basis of the data shown in Figure 1 is a Rietveld analysis of the crystalline phases in the respective diffractograms, finally plotted as relative fraction of the ZrO_2 phases versus annealing temperature. The X-ray diffractograms are shown in Figure S2 in the Supporting Information, as is a corresponding exemplary Rietveld analysis (Supporting Information, Figure S1). As shown in panel A, crystallization of the tetragonal ZrO_2 phase sets in fast and is finished at 400 °C. No tetragonal ZrO_2 is observed below 400 °C, and once crystallized, no remaining amorphous ZrO_2 is qualitatively visible in the background of the XRD patterns at annealing temperatures of 400 °C and above. No apparent crystallization of the monoclinic phase has been observed over the entire period of the experiment. Repeating the experiment, but annealing to 600, 800, and 1000 °C, causes reproducible presence and detection of the tetragonal phase at 400 °C but also induces further partial transformation of the tetragonal into the monoclinic phase. Up to 20% of this latter phase is found in the product mixture at the respective highest temperatures. Upon recooling, this amount increases without exception up to 80–90%.

To further shed light on the kinetics of the transformation from tetragonal to monoclinic ZrO_2, the enrichment of monoclinic ZrO_2 in the product mixture was analyzed as a function of reaction time during annealing/the isothermal periods and plotted as shown in Figure 2. The vertical lines

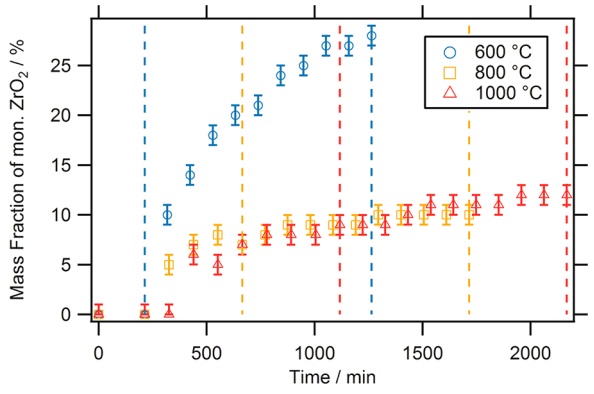

Figure 2. Kinetic analysis of the tetragonal-to-monoclinic phase transformation as a function of annealing time and temperature shown as enrichment of the crystalline monoclinic ZrO_2 phase during annealing/the isothermal reaction parts. Experiments up to 600, 800, and 1000 °C are represented on the basis of the data highlighted in Figure 1 (heating rate < 0.01 °C s^{-1}). The dashed vertical lines represent the isothermal reaction parts after annealing. Duration of the isothermal periods as in Figure 1.

limit the respective isothermal periods. Note that the temperature information can in principle be extracted directly from the time axis: hence, the second point at 213 min of reaction time corresponds to 600 °C. Consequently, the onset of formation of the monoclinic phase is observed roughly at the same temperature of ~600 °C. However, the subsequent transformation rate during the subsequent isothermal periods and/or annealing to higher temperatures is clearly different. A steep increase of the amount of monoclinic ZrO_2 after prolonged heating for 1 h at 600 °C is observed, adding up to about 30 wt % at the end of reaction. The formation of the monoclinic ZrO_2 phase is apparently not finished at 1263 min of reaction time (red dashed line). In contrast, either heating to and holding the temperature at 800 or 1000 °C clearly slows the phase transformation rate to monoclinic ZrO_2, and in consequence, at maximum only 10% monoclinic ZrO_2 is observed. These differences are most clearly seen in the isothermal reaction periods.

To unravel the kinetics of the tetragonal-to-monoclinic phase transformation in more detail, associated experiments with a comparably fast heating rate (0.5 °C s^{-1}) were additionally performed (Figure 3; the corresponding XR diffractograms are

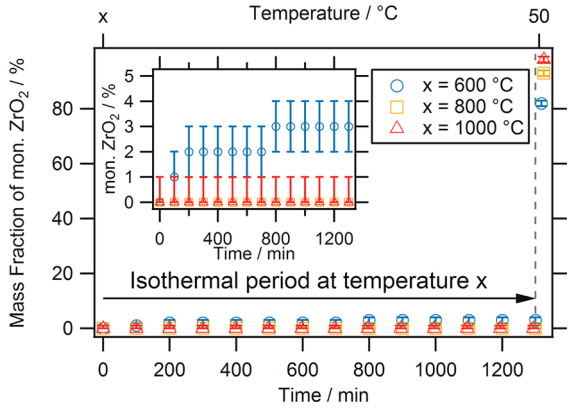

Figure 3. Kinetic analysis of the tetragonal-to-monoclinic phase transformation as a function of reaction time at 600, 800, and 1000 °C shown as enrichment of the crystalline monoclinic ZrO_2 phase as for the fast XRD heating experiments (0.5 °C s^{-1}). (inset) An expanded view. Isothermal period: 23 h 20 min.

shown in Supporting Information, Figure S3). Obviously, the extent of phase transformation in the isothermal reaction parts is very much suppressed in comparison to the data shown in Figure 2—at maximum, 3% monoclinic ZrO_2 was observed after annealing at 600 °C. Also in accordance with Figure 2, the amount of monoclinic ZrO_2 formed at higher temperatures is much lower. For the experiments highlighted in Figure 3, at 800 and 1000 °C no visible phase transformation has taken place. In contrast, but corroborating the data shown in Figure 2, after recooling to room temperature, the associated phase transformation is almost complete (80–100% monoclinic ZrO_2). This indicates that the major part of the phase transformation occurs during cooling.

A particularly important topic in catalysis, especially with respect to a potential use in reforming reactions, is the metastability under moist conditions (in the presence of water vapor as a reactant). In this respect, Xie et al. report a significantly faster rate of the tetragonal-to-monoclinic transformation in the presence of water vapor, even at room temperature. As a tentative explanation, altered surface free energies of monoclinic and tetragonal ZrO_2 with and without water adsorbed on their surfaces, and moreover, as a function of crystallite size, is offered.[35] In due course, we tested our tetragonal ZrO_2 phase for its stability under moist conditions in the temperature range from room temperature to 420 °C. For these experiments, the tetragonal ZrO_2 phase was crystallized by annealing in dry oxygen up to 420 °C, recooled to room

dx.doi.org/10.1021/ic502623t | Inorg. Chem. 2014, 53, 13247–13257

temperature, and finally treated in moist He in the above-mentioned temperature range for 1 h. All samples were annealed and recooled in moist He. The corresponding XR diffractograms are summarizingly shown in Figure 4. It is

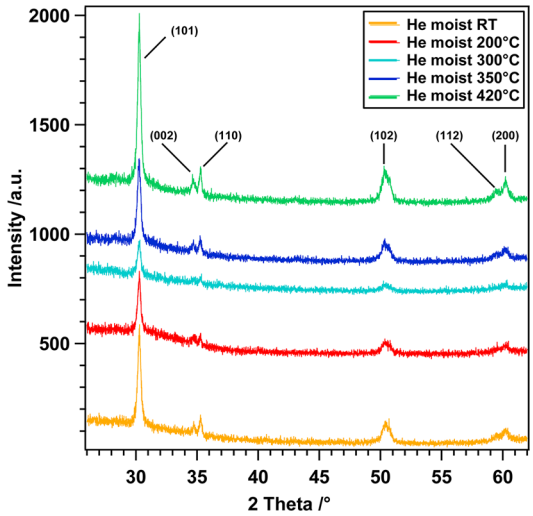

Figure 4. X-ray diffractograms collected after treatment of the tetragonal ZrO_2 phase in moist He at temperatures from room temperature (25 °C) to 420 °C. He was saturated with water vapor (6.1 mbar), and the sample was heated and recooled under moist conditions. The total flow was ~1 mL s^{-1}. Reflections of the tetragonal ZrO_2 structure were indexed according to ref 39.

immediately clear that only tetragonal ZrO_2 is present, and no transformation into the monoclinic phase was observed. (Indexing of the reflections of the tetragonal phase was based on pattern No. 00−050−1089 for Cl^--stabilized ZrO_2, PDF 4+ database.[39])

Analogous experiments were also performed for the corresponding Y-doped ZrO_2 sample. As a representative example, the heating−isothermal period−recooling cycle from room temperature to 1000 °C is shown (Figure 5). As can be clearly seen, the initially amorphous Y-doped ZrO_2 sample

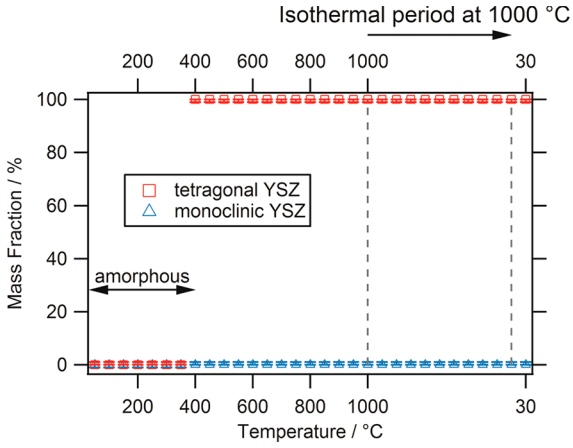

Figure 5. Representation of the high-temperature X-ray diffraction experiments on the Y-doped ZrO_2 sample after annealing up to 1000 °C. The colors of the markers denote the different tetragonal and monoclinic ZrO_2 phases. Dashed vertical lines indicate the range of the isothermal period (18 h 20 min). The arrow indicates the presence range of amorphous ZrO_2.

crystallizes in the tetragonal ZrO_2 structure but persists in further transformation to a monoclinic phase at any temperature, in contrast to pure ZrO_2. The corresponding patterns are shown in Figure S4 in the Supporting Information.

3.2. In Situ Transmission Electron Microscopy and Scanning Electron Microscopy. Figures 6 and 7 show the in

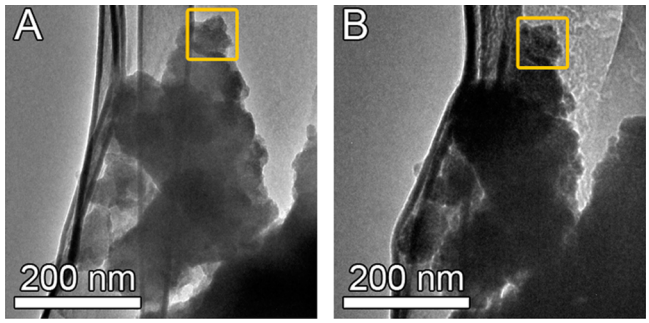

Figure 6. Overview transmission electron micrographs of the pure ZrO_2 sample before (A) and after (B) the heating−cooling cycle. The square-marked region is shown in high-resolution detail in Figure 7.

situ electron microscopy experiments performed to monitor the structural evolution during the annealing in close correlation to the X-ray diffraction and the thermogravimetric analysis. We, however, note that due to the experimental conditions during annealing of the sample using the TEM heating stage, the heating rate is very fast (comparable to TGA, but much faster than during the "slow" high-temperature XRD experiments). Comparing the TEM overview images of a ZrO_2 grain before (i.e., in the amorphous state, Figure 6A) and after the annealing treatment up to 900 °C (Figure 6B), the crystallization is clearly visible by the enhanced internal contrast of the grain within the square-marked region, which is indicated in both images and refers to the area that was monitored during the annealing experiment shown in Figure 7. Figure 7 finally shows the SAED patterns and the high-resolution images acquired during the in situ annealing treatment. (The full assignment of the measured reflections to theoretical lattice spacings is outlined in Table S2 in the Supporting Information.) The full sequence of the experiment from room temperature to 900 °C and back to room temperature is highlighted in panels A−H (characteristic reflections of the tetragonal ZrO_2 structure are marked in blue, those of the monoclinic structure in orange). In the gel precursor state (panels A and B) the structure is amorphous, as evidenced in the SAED pattern showing only a diffuse halo and the high-resolution image, where no lattice fringes or any other signs of crystallization are present. In accordance with XRD and thermogravimetry, crystallization of the tetragonal ZrO_2 phase occurs at ~400 °C (panels C and D). The distinct tetragonal SAED pattern, as well as the corresponding lattice fringes, are observed in the high-resolution images (some of the most intense reflections and most characteristic fringes are marked). Up to 750 °C, no intensity changes in the reflections of the tetragonal ZrO_2 structure or any additional spots/fringes in the corresponding SAED patterns or TEM images were observed. However, at higher temperatures, especially the SAED patterns indicate the formation of modest amounts of the monoclinic ZrO_2 phase (panels E and F). This phase also persists upon recooling the sample (panels G and H), but its amount does not increase substantially. The presence of the monoclinic ZrO_2 phase was

dx.doi.org/10.1021/ic502623t | Inorg. Chem. 2014, 53, 13247−13257

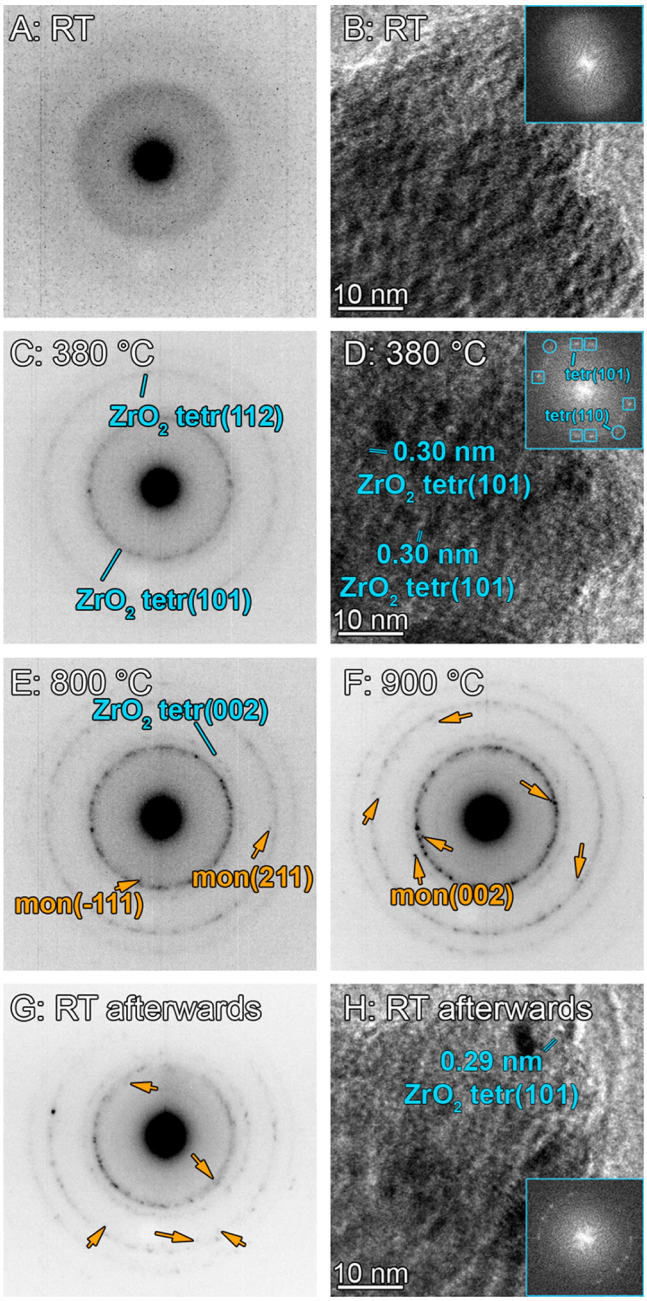

Figure 7. In situ collected transmission electron microscopic images following the crystallization of the ZrO_2 phases from room temperature to 900 °C, as well as after recooling to room temperature. Important reflections of the tetragonal (blue) and monoclinic ZrO_2 phase (orange) were marked. Orange arrows in panels F and G denote reflections of the monoclinic structure, corresponding to the listing in the Supporting Information, Table S2. Temperatures were as indicated.

inferred by the appearance of very weak additional spots in the SAED pattern (corresponding to the (−111) and (211) reflection of the monoclinic ZrO_2 structure, pattern No. 00−037−1484, PDF 4+ database,[42] panel E). We emphasize that not only the stability of the phase-pure tetragonal ZrO_2 sample up to 750 °C but also the essential phase-purity at higher temperatures and upon recooling is basically due to the fast heating and cooling rates, which suppress the further transformation into the monoclinic phase. Also note that the electron microscopy data, especially those after recooling the sample to room temperature in vacuo, in fact corroborate the suggestions by different authors, that the oxygen/water partial pressure and the resulting vacancy concentration upon recooling dominates the eventual phase transformation from tetragonal to monoclinic ZrO_2. Samples cooled in vacuo—due to the higher amount of vacancies and the resulting better structural stability of tetragonal ZrO_2—are suggested to persist during the transformation into the monoclinic modification. In contrast, the higher the amount of oxygen/water, the faster the transformation into monoclinic ZrO_2.[27,29,30,35] In our experiments, the amount of monoclinic ZrO_2 is accordingly very low. This is basically corroborated especially by the thermogravimetric analysis and again proves that the stability is very much dominated by surface chemistry-induced kinetic effects.

The morphology of the samples after different annealing steps was additionally followed by scanning electron microscopy and corroborates the loss of surface area during annealing to very high temperatures. The images are shown in Figure S5 in the Supporting Information.

3.3. Thermogravimetric Analysis. To exactly determine the temperature of the eventual phase transformations and to gain associated information on the chemical changes during the phase transformation, thermogravimetric analysis coupled with mass spectrometry was performed. These experiments included also time- and rate-dependent measurements to investigate the kinetic limitations of the phase transformation(s).

Figure 8 highlights experiments using a rather fast heating rate of 0.25 °C min^{-1} up to 600 °C with immediate recooling to room temperature. The black trace (in panel A) denoting the mass loss during annealing indicates that most of the mass loss, totalling 2.8 mg (corresponding to 18%), is happening up to ∼300 °C, well before crystallization to tetragonal ZrO_2 takes place. The first (and only) transformation is observed at ∼400 °C (strong exothermic peak in the blue trace). Also upon recooling, no other transformation is observed. As evidenced by HT-XRD and in situ TEM, the phase transformation can be correlated with the crystallization of the tetragonal ZrO_2 modification. No monoclinic structure was observed during this experiment. The mass spectrometer signals (panels B and C) indicate mostly loss of water (m/z = 18), CO_2 (m/z = 44), CO (m/z = 28) and CH-containing fragments arising from the decomposition of the isopropoxide alkyl group (m/z = 58, 59, 60). Most notably, all chemical changes are clearly finished before the amorphous-to-tetragonal ZrO_2 transformation sets in. Together with XRFA and the results from the structural analysis, we might infer the presence of a chemically and phase-pure tetragonal ZrO_2 sample after annealing to 400 °C and also after recooling to room temperature.

To investigate the kinetic stability of the tetragonal structure, a corresponding experiment with a comparable heating rate (1 °C min^{-1}), but an extended isothermal period at 600 °C for 6 h, was performed and is shown in Figure 9. As can be clearly seen, also in this case, no further transformation into the thermodynamically more stable monoclinic polymorph was observed. In summary, the decomposition of the gel precursor state appears to be finished at ∼300 °C, followed by crystallization of the tetragonal ZrO_2 structure at ∼400 °C. In-between, amorphous ZrO_2 is present, without signs of crystallization.

3.4. Raman Spectroscopy. To finally gain spectroscopic insight into the phase formation, Raman spectra were collected for various samples after different decomposition/crystallization and annealing treatments. The corresponding spectra are

dx.doi.org/10.1021/ic502623t | Inorg. Chem. 2014, 53, 13247−13257

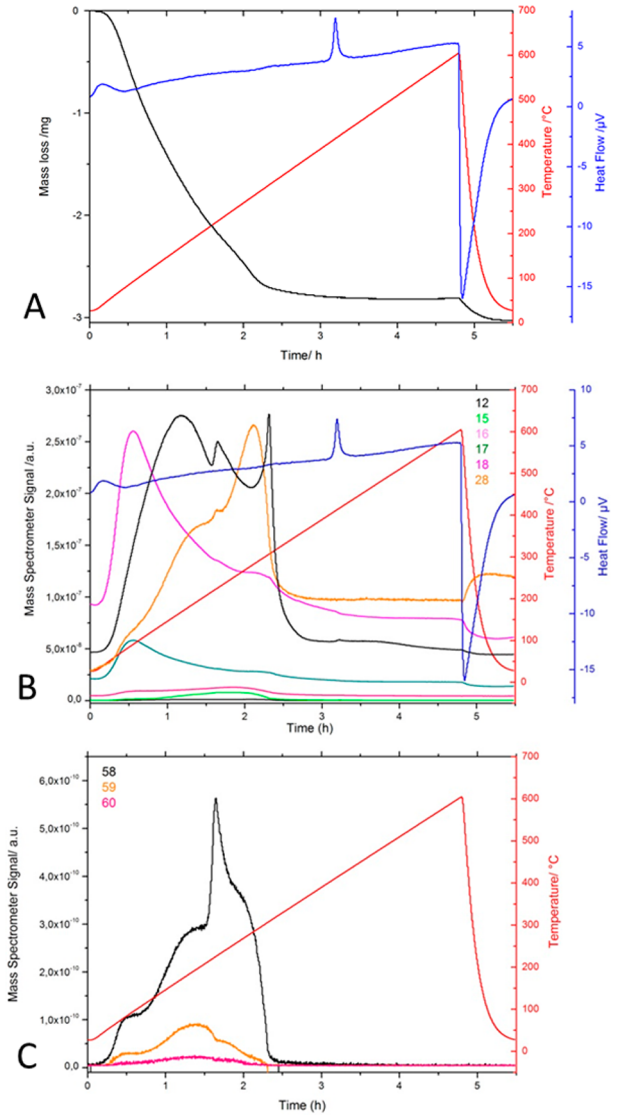

Figure 8. Thermogravimetric analysis of the ZrO_2 gel precursor state during its decomposition/crystallization of the tetragonal ZrO_2 phase. (A) Mass loss (black trace) and heat flow (blue trace) vs annealing temperature (red trace). Heating rate: 0.25 °C min^{-1}. (B) Mass spectrometer signals of CO_2 (m/z = 44, black), water (m/z = 15,16,17, and 18; green, dark yellow, magenta, and lilac), and CO (m/z = 28; orange) including heat flow and annealing temperature. (C) Mass spectrometer signals resulting from the decomposition of the alkyl groups (m/z = 58, 59, and 60) including annealing temperature.

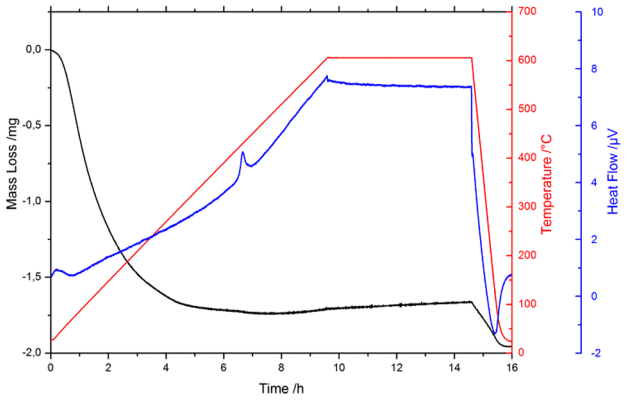

Figure 9. Thermogravimetric analysis of the ZrO_2 gel precursor state during its decomposition/crystallization of the tetragonal ZrO_2 phase with extended isothermal period at 600 °C. Mass loss (black trace) and heat flow (blue trace) vs annealing temperature (red trace). The heating rate was set to 1 °C min^{-1}.

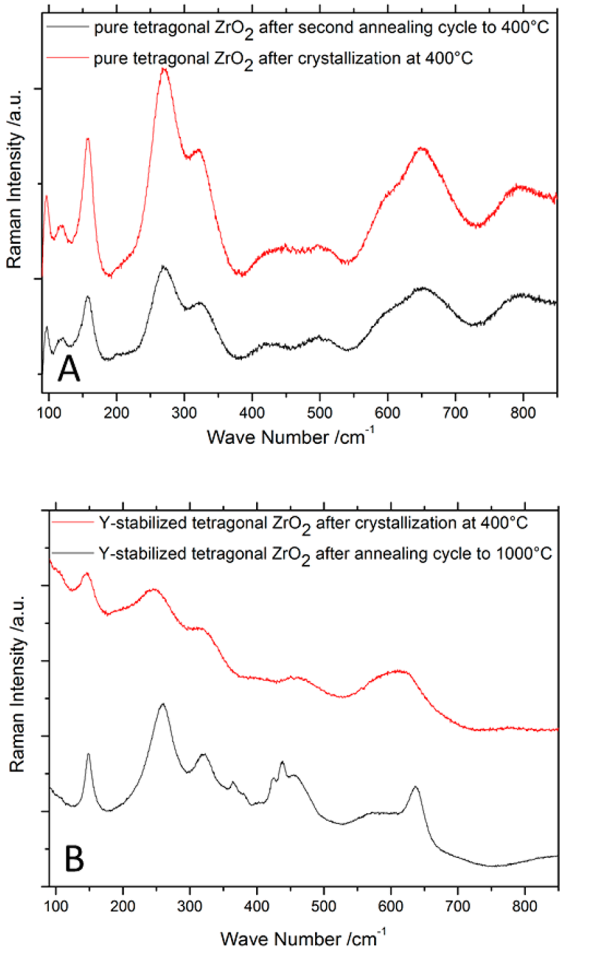

Figure 10. Raman spectra collected on the pure tetragonal ZrO_2 (A) and the Y-stabilized ZrO_2 phase (B) after crystallization at 400 °C and after corresponding second annealing cycles to 400 and 1000 °C, respectively.

shown in Figure 10. Panel A highlights the experiments on pure tetragonal ZrO_2; panel B highlights those on the corresponding Y-stabilized phase. In accordance with literature-reported spectra, both the Raman spectra taken after crystallization at 400 °C and after the corresponding annealing cycle match the typical fingerprints of the tetragonal structure found after annealing hydrous ZrO_2 precursors arising from chloride-containing solutions.[43,44] Note that group analysis predicts six Raman-active vibrational modes for tetragonal ZrO_2, which were also shown experimentally.[45,46] Figure 10A, however, exhibits at least 10 distinguishible peaks. This could in principle be explained by the presence of a monoclinic ZrO_2 phase (from an eventual phase transformation, yielding 18 additional vibrational modes[47]), which has not been detected in XRD measurements (cf. Figure 1). More likely is a symmetry breaking by disordering phenomena or hydrous compounds arising from the preparation process. As the course of the two spectra does not change considerably, we might infer a high structural stability of pure tetragonal ZrO_2 in this temperature regime. A slightly different behavior was observed for the

dx.doi.org/10.1021/ic502623t | Inorg. Chem. 2014, 53, 13247−13257

corresponding Y-doped tetragonal ZrO_2 structure (Figure 10B). Compared to the spectrum after crystallization, the one obtained after the annealing cycle to 1000 °C exhibits many more details, especially in the region between 300 and 500 cm^{-1}. The red spectrum is in good agreement with those reported in literature for Y-doped ZrO_2.[48] Note that, to explain the details found in the black spectrum of Figure 10B, contributions from symmetry breaking and/or presence of hydrous compounds must also be assumed, as no monoclinic phase was detected in the corresponding X-ray diffractograms, in close correlation with the experiments on pure tetragonal ZrO_2. This is highly likely, given the comparable preparation process.

4. DISCUSSION

4.1. Preparation Aspects. As the phase stability and specific surface area is of paramount importance especially for the use as catalytic material or catalyst support, lots of effort has been placed in opening new preparation pathways to single-phase cubic, tetragonal, and monoclinic ZrO_2 with a high specific surface area. Starting materials are usually solutions of zirconium/zirconyl salts and various alkoxide derivatives, which are hydrolyzed to obtain the corresponding oxide material.[5,7,9,15−31,34] Following this routine, all three ZrO_2 polymorphic modifications could be obtained, albeit exhibiting different particle sizes, morphologies, structures, and kinetic stabilities.[5,12,17,22,32] Focusing on the tetragonal structure, as reasons for the enhanced kinetic stability of thermodynamically metastable tetragonal ZrO_2, intrinsic size effects (stabilizing the tetragonal structure below a critical particle diameter),[8] presence of defects in the final oxide matrix[9,21,24,25,27] or structural similarities between the amorphous precursor structure and tetragonal ZrO_2 species have been discussed.[5,8,33,34] However, especially regarding zirconium alkoxide decomposition (but not limited to), the influence of the experimental conditions on the structural stability is significant and encompasses the chemical nature of the alkyl group, solvent, postannealing temperature, and oxygen and water partial pressures or pH value, among others.[15,16,18−22] However, for a useful the preparation routine, one major drawback remains: because of the inherent metastability of tetragonal ZrO_2, both the primary preparation of this structure as a single phase, as well as its structural stability upon annealing, or during its specific application, is far from being straightforward. Usually, either mixtures of tetragonal and monoclinic ZrO_2 (with the former usually as the major component) right after preparation or a partial or full transformation into the monoclinic structure upon annealing to 1000 °C are reported. Inoue et al. state a stability range of the tetragonal structure from 300 to 700 °C.[18] These authors also performed a thorough investigation of the influence of the alkyl group and the solvent on the resulting ZrO_2 structure, and although single-phase tetragonal ZrO_2 resulted directly after preparation, annealing to 500 °C without exception introduced varying amounts of monoclinic ZrO_2.[16] Similar results, albeit at different temperatures, were also reported by Mazdiyasni et al.[15] Comparable experimental results are obtained upon polymerization of zirconium alkoxide precursors.[20] Collins et al. reported a time-dependent stability of tetragonal ZrO_2 at 900 °C (for 12 h), before subsequent transformation into the monoclinic modification.[22] Jung et al. reported the formation of tetragonal ZrO_2 (synthesized from zirconyl chloride), structurally stable up to 900 °C, synthesized at pH 10, and followed by prolonged treatment in the mother liquor at 100 °C.[47] Valuable input into the stability of the tetragonal ZrO_2 phase and its stability is also provided by the works of Stefanic et al. and related to the influence of the oxygen partial pressure and the presence of cationic and anionic stabilizers.[24,29,31] Structural stability of the tetragonal ZrO_2 phase has been verified by high-temperature X-ray diffraction up to 1200 °C.[29] Two notable differences to the experimental features of our work should be noted. First, the heating rate in the latter work amounted to 5 °C min^{-1}, which is about 500 times faster than reported in the "slow" experiments in our work. This would in turn nicely fit to the kinetic limitations discussed here and would explain why (except for the experiment up to 400 °C), in our case, for much lower heating rates increasing amounts of monoclinic ZrO_2 are observed. In case of higher heating rates, as, for example, in the TEM, TGA, or additional XRD experiments, no or only modest amounts of monoclinic ZrO_2 are observed.

More critical, however, appears to be the use of the zirconyl nitrate and zirconyl chloride as precursor materials to prepare the tetragonal phase.[24,29,31,43,44] Consequently, as remaining nitrate or chloride ions are known to additionally aid the stabilization of the tetragonal phase,[27] the resulting samples might be better viewed as representatives of doped or externally ionically stabilized tetragonal ZrO_2 phases.

4.2. Overview of Phase Transformations from Tetragonal to Monoclinic ZrO_2. Mixtures of tetragonal and monoclinic ZrO_2 phases have been explicitely stated by Chang et al. (following a sol−gel hydrolyzation synthesis method starting from $ZrCl_4$; phase transformation tetragonal → monoclinic at 550 °C),[27] Srinavasan et al. (starting from $ZrCl_4$; phase transformation tetragonal → monoclinic at 500 °C),[28] Mazdiyasni et al. (starting from Zr alkoxide precursors; phase transformation tetragonal → monoclinic at 300 °C),[15] Inoue et al. (starting from Zr *n*-propoxide; phase transformation tetragonal → monoclinic at 450 °C),[18] Inoue et al. (starting from Zr *n*-propoxide; phase transformation tetragonal → monoclinic at 700 °C, depending on organic solvent),[16] Collins (starting from dibutoxy(acetylacetonato) zirconium, phase transformation tetragonal → monoclinic during annealing to 700 °C),[19,21] Hertl (starting from Zr 1-propoxide; phase transformation tetragonal → monoclinic during annealing to 500 °C in air),[49] Jung et al. (starting from zirconyl chloride; phase transformation tetragonal → monoclinic during annealing to 500 °C depending on the pH value and synthesis conditions),[50] and Oleshko et al. (starting from Zr n-propoxide; phase transformation tetragonal → monoclinic at 400 °C).[5] Especially the latter is a very important work, since it provides a detailed HRTEM study of an allegedly phase-pure, unstabilized tetragonal ZrO_2 phase. In this case, stabilization of the tetragonal structure is reported to be related to a particle size effect. An important factor in stabilization of the tetragonal modification also refers to the number of oxygen vacancies and surface hydroxyl groups during preparation. Dehydroxylation and deoxygenation are reported to generally favor the stabilization of the tetragonal phase.[27]

4.3. Discussion of the Stability of the Tetragonal ZrO_2 Phase. Putting these data into perspective of our own work, we might infer a combination of a particle size and vacancy effects, leading to enhanced stabilization of the tetragonal ZrO_2 phase. Regarding the particle size effect, the mean particle diameter up to ∼100 nm is well in the range of that reported by Oleshko et al. being necessary for stabilization of tetragonal ZrO_2.[5] Additionally, the chosen preparation pathway ensures that at

dx.doi.org/10.1021/ic502623t | Inorg. Chem. 2014, 53, 13247−13257

the beginning of the precipitation of the gel precursor, small particles with an associated high density of defects are present, also aiding the stabilization. The further fate of the tetragonal phase is in due course very much dominated by kinetic limitations. Unfortunately, in most literature-reported cases, the heating or annealing rates are not explicitly stated, rendering a direct comparison of the dependence on the kinetics of phase transformation difficult. If stated, as, for example, in the paper by Stefanic et al.,[24] the results clearly corroborate the stability characteristics stated here. We note that also related to the kinetics of phase transformation, the amount of monoclinic ZrO_2 without exception drastically increases upon recooling to room temperatures from 10 to 20% up to ∼80%. Similar observations have also been made by Stefanic et al.[25] who additionally concluded that oxygen aids the transformation, since samples cooled in vacuo and finally exposed to air at room temperature exhibited a much higher amount of tetragonal ZrO_2 compared to samples cooled in air. Additionally, we might also infer an influence of stress relief during heating and cooling. The phase transformation from tetragonal to monoclinic ZrO_2 is long known to be associated with the appearance of distinct cracks in the structure, along which the phase transformation predominantly proceeds.[2] Consequently, we might on the one hand expect stress relief at higher temperatures due to thermal healing of these defects, while on the other hand, upon recooling, the stress is finally relieved by accelerated transformation into the thermodynamically more stable monoclinic structure. This has been investigated also recently by theoretical phase-field modeling.[51] These calculations also suggest the experimentally observed slowing of the phase transformation at higher annealing temperatures, as shown in Figures 2 and 3. Also this behavior could be explained by the above-discussed thermal healing of stress at higher temperatures (i.e., 800 and 1000 °C), which is clearly absent at lower annealing temperatures (i.e., 600 °C). As for the kinetics of the phase transformation from tetragonal to monoclinic ZrO_2, isothermal experiments have been conducted by Zhu et al. for a number of tetragonal samples stabilized by 2 mol % Y_2O_3.[52,53] In these works, the importance of oxygen vacancies has been stressed. In addition, these authors also observed a characteristically "nose"-shaped time−temperature-dependent curve, which essentially indicates that the transformation rate proceeds through a maximum at a distinct temperature, which has been determined to be 300 °C. This is directly related to the work described herein, where also a characteristic temperature (i.e., 600 °C) was revealed, where the transformation rate particularly accelerates. Note, however, that the major difference between the two works is the use of pure tetragonal versus Y-stabilized ZrO_2.

4.4. Stability of the Tetragonal ZrO_2 Phase under Moist Conditions. A particularly important topic, which is of paramount importance for the use as catalytic material, refers to the stability under moist conditions. This has been in detail only studied by Xie et al.,[35] who found that tetragonal ZrO_2 under moist conditions undergoes a transformation to monoclinic ZrO_2—at room temperature and as a consequence of energetic reasons due to adsorbed water. This, of course, would consequently exclude the use of tetragonal ZrO_2 from all reforming reactions (e.g., including methanol or methane). On top of that, the BET surface of this reported tetragonal ZrO_2 sample amounted to ∼100 $m^2\ g^{-1}$, that is, very small particles, well-inside the stability range reported by other authors, were present. In contrast, our tetragonal sample clearly not only persists during the transformation to monoclinic ZrO_2, even under moist experimental conditions, but—as deduced from BET measurements—the specific surface area is lower by a factor of 10. This might indicate a higher stability for even larger particles. As a consequence, the influence of water also affects the recooling of the sample. Here, up to now, the oxygen partial pressure has been solely held accountable for the reduced stability if the sample was cooled in air. In the light of the results by Xie et al. and the data presented in this work, water must be equally considered as a potential source of phase transformation. This cannot be directly extracted from our work, since the stability both under dry and moist conditions has been only verified up to 420 °C. This, however, is well in the temperature range of, for example, methanol reforming reactions. These considerations would consequently refer to all experiments, where recooling has been stated to proceed under ambient conditions.[24]

4.5. The Effect of Stability on Characterization and Application of Tetragonal ZrO_2. More critical, however, is that this discussed temperature- and time-dependent stability in turn poses great difficulties regarding characterization of the tetragonal phase. In that respect, a number of characterization studies of tetragonal ZrO_2 have been published, especially regarding adsorption of small probe molecules such as CO/CO_2 and the resulting surface acid/base surface properties.[12−14,54] However, some of the so-called "pure" tetragonal ZrO_2 phases reported in these contributions are either stabilized with 3.5% SiO_2[13] or even 3% Y_2O_3 (despite being named pure tetragonal ZrO_2).[14,54] In some cases, the initial sample was clearly structurally pure tetragonal ZrO_2, but—despite annealing to 600 °C—its structural integrity was not reported after use.[12] As a consequence, the chemical, structural, electronic, and adsorption properties of the pure tetragonal ZrO_2 modification appear to be still grosso modo unknown.

5. CONCLUSIONS

This study shows the importance of not only adequate preparation techniques but also the accurate control of postpreparation experimental conditions to access structurally stabilized pure oxidic materials. "Pure" in this respect refers to both the absence of possible obvious ionic stabilizers (such as nitrate or chloride but also stabilizing cationic species) already in the precursor state and to the structural stability upon annealing/recooling. In due course, the stabilization of the tetragonal structure by Y itself is not an unexpected result. However, the chosen preparation routine by simultaneous precipitation of hydrous ZrO_2 and Y_2O_3 aerogels and the subsequent apparent formation of a Y-doped amorphous aerogel, finally yielding Y-stabilized tetragonal ZrO_2, is important insofar as it allows both a very simple chemical pathway to this oxide polymorph and the possibility to directly compare essentially pure and Y-doped tetragonal ZrO_2. Thus, this will eventually reveal different materials or adsorption properties and would allow to also judge literature-reported data and assess the influence of a potentially unwanted introduction of monoclinic ZrO_2. Particularly important in oxide chemistry is the chemical state of a material's surface, which steers adsorption properties and obviously also crucially influences the stability of bulk structures, at least in the ZrO_2 system. Therefore, accurate control, especially of the hydroxylation degree of the surface, is of paramount importance and needs to be separately assessed in future directional in situ FT-IR spectroscopy experiments. This

especially refers to the influence of water and clarifying, which triggers the transformation into the monoclinic structure upon recooling the tetragonal ZrO_2 phase, which was calcined at very high temperatures ($T \geq 600$ °C). We have shown the preparation of a chemically pure, structurally stable tetragonal ZrO_2 phase, which can now be in detail characterized up to temperatures of ∼450 °C; future work will reveal the intrinsic structural, electronic, adsorption, and catalytic properties of pure tetragonal ZrO_2, in comparison to both monoclinic and Y-stabilized ZrO_2.

■ ASSOCIATED CONTENT

Supporting Information

Chemical analyses, exemplary Rietveld analysis, and X-ray diffraction patterns, as well as scanning electron microscopic images and SAED analysis. This material is available free of charge via the Internet at http://pubs.acs.org.

■ AUTHOR INFORMATION

Corresponding Author

*E-mail: simon.penner@uibk.ac.at. Phone: 004351250758003. Fax: 004351250758199.

Author Contributions

⊥These two authors contributed equally to the work.

Notes

The authors declare no competing financial interest.

■ ACKNOWLEDGMENTS

We thank the FWF (Austrian Science Foundation) for financial support under Project No. F4503−N16. All experiments were performed within the framework of the platform "Advanced Materials" at the University of Innsbruck. We are indebted to K. Pfaller for assistance with scanning electron microscopy.

■ REFERENCES

(1) Lee, J. H. *J. Mater. Sci.* **2003**, *38*, 4247−4257.
(2) Rühle, M. *Adv. Mater.* **1997**, *9*, 195−217.
(3) Garnweitner, G. Zirconia Nanomaterials: Synthesis and Biomedical Applications. In *Nanotechnologies for the Life Sciences;* Kumar, C., Ed.; Wiley-VCH: Weinheim, Germany, 2007.
(4) Han, Y.; Zhu, J. *Top. Catal.* **2013**, *56*, 1525−1541.
(5) Oleshko, V. P.; Howe, J. M.; Shukla, S.; Seal, S. *J. Nanosci. Nanotechnol.* **2004**, *7*, 867−875.
(6) Badwal, S. P.; Bannister, M. J. *Science and Technology of Zirconia V;* Technomic Publishing Co.: Lancaster, PA, 1993.
(7) Shukla, S.; Seal, S.; Vij, R.; Bandyopadhy, S.; Rahman, Z. *Nano Lett.* **2002**, *2*, 989−993.
(8) Garvie, R. *J. Phys. Chem.* **1965**, *69*, 1238−1243.
(9) Livage, J.; Doi, K.; Mazieres, C. *J. Am. Ceram. Soc.* **1968**, *51*, 349−353.
(10) Porter, D. L.; Evans, A. G.; Heuer, A. H. *Acta Metall.* **1979**, *27*, 27−35.
(11) Menzler, N. H.; Tietz, F.; Uhlenbruck, S.; Buchkremer, H. P.; Stöver, D. *Mater. Sci.* **2010**, *45*, 3109−3135.
(12) Pokrovski, K.; Jung, K.; Bell, A. T. *Langmuir* **2001**, *17*, 4297−4303.
(13) Bachiller-Baeza, B.; Rodriguez-Ramos, I.; Guerrero-Ruiz, A. *Langmuir* **1998**, *14*, 3556−3564.
(14) Bolis, V.; Magnacca, G.; Cerrato, G.; Morterra, C. *Thermochim. Acta* **2001**, *379*, 147−161.
(15) Mazdiyasni, K. S.; Lynch, C. T.; Smith, J. S. *J. Am. Chem. Soc.* **1965**, *49*, 286−287.
(16) Inoue, M.; Kominami, H.; Inui, T. *Appl. Catal., A* **1995**, *121*, L1−L6.
(17) Chatterjee, A.; Pradhan, S. K.; Datta, A.; De, M.; Chakravorty, D. *J. Mater. Res.* **1994**, *9*, 263−265.
(18) Inoue, M.; Kominami, H.; Inui, T. *Appl. Catal., A* **1993**, *97*, L25−L30.
(19) Collins, D. E.; Brown, K. J. *J. Mater. Res.* **1998**, *13*, 1230−1237.
(20) Yoldas, B. E. *J. Mater. Sci.* **1986**, *21*, 1080−1086.
(21) Collins, D. E.; Rogers, K. A.; Bowman, K. J. *J. Eur. Ceram. Soc.* **1995**, *15*, 1119−1124.
(22) del Monte, F.; Larsen, W.; Mackenzie, J. D. *J. Am. Ceram. Soc.* **2000**, *83*, 6228−6234.
(23) Matero, R.; Ritala, M.; Leskelä, M.; Jones, A. C.; Williams, P. A.; Bickley, J. F.; Steiner, A.; Leedham, T. J.; Davies, H. O. *J. Non-Cryst. Solids* **2002**, *303*, 24−28.
(24) Stefanic, G.; Grzeta, B.; Popovic, S.; Music, S. *Croat. Chem. Acta* **1999**, *72*, 395−412.
(25) Osendi, M.; Moya, J.; Serena, C.; Sora, J. *J. Am. Ceram. Soc.* **1985**, *68*, 135−139.
(26) Mamott, G. T.; Barnes, P.; Tarling, S. E.; Jones, S. L.; Norman, C. J. *Powder Diffr.* **1988**, *3*, 234−239.
(27) Chang, S.; Doong, R. *Chem. Mater.* **2005**, *17*, 4837−4844.
(28) Srinivasan, R.; Davis, B. H.; Cavin, O. B.; Hubbard, C. R. *J. Am. Ceram. Soc.* **1992**, *75*, 1217−1222.
(29) Davis, B. H. *J. Am. Ceram. Soc.* **1984**, *67*, C−168.
(30) Stefanic, G.; Music, S.; Grzeta, B.; Popovic, S.; Sekulic, A. *Croat. Chem. Acta* **1998**, *71*, 789−806.
(31) Stefanic, G.; Music, S.; Popovic, S.; Furic, K. *Croat. Chem. Acta* **1996**, *69*, 223−239.
(32) Thalinger, R.; Stöger-Pollach, M.; Hetaba, W.; Feuerbacher, M.; Klötzer, B.; Penner, S. *Mater. Chem. Phys.* **2013**, *143*, 167−177.
(33) Kasatkin, I.; Girgsdies, F.; Ressler, T.; Caruso, R. A.; Schattka, J. H.; Urban, J.; Weiss, K. *J. Mater. Sci.* **1995**, *30*, 2151−2157.
(34) Tani, E.; Yoshimura, M.; Somiya, A. *J. Am. Ceram. Soc.* **2006**, *66*, 11−14.
(35) Xie, S.; Iglesia, E.; Bell, A. T. *Chem. Mater.* **2000**, *12*, 2442−2447.
(36) Bruker AXS. *DIFFRAC^{plus} EVA,* Version 19; Bruker AXS: Karlsruhe, Germany, 2013.
(37) *PDF-4+;* International Centre for Diffraction Data (ICDD): Newtown Square, PA, 2013.
(38) Bruker AXS. *TOPAS V4,* General profile and structure analysis software for powder diffraction data.—Users Manual; Bruker AXS: Karlsruhe, Germany, 2008.
(39) Malek, J.; Benes, L.; Mitsuhashi, T. *Powder Diffr.* **1997**, *12*, 96−98.
(40) Yashima, M.; Sasaki, S.; Kakihana, M.; Yamaguchi, Y.; Arashi, H.; Yoshimura, M. *Acta Crystallogr., Sect. B* **1994**, *50*, 663−672.
(41) Yashima, M.; Hirose, T.; Katano, S.; Suzuki, Y.; Kakihana, M.; Yoshimura, M. *Phys. Rev. B* **1995**, *51*, 8018−8025.
(42) McMurdie, H. F.; Morris, M. C.; Evans, E. H.; Paretzkin, B.; Wong-Ng, W.; Ettlinger, L.; Hubbard, C. R. *Powder Diffr.* **1986**, *1*, 265−275.
(43) Mercera, P.D. L.; Van Ommen, J. G.; Doesburg, E. B. M.; Burggraaf, A. J.; Ross, J. R. H. *Appl. Catal.* **1990**, *57*, 127−148.
(44) Srinavasan, R.; Harris, M. B.; Simpson, S. F.; DeAngelis, R. J.; Davis, B. H. *J. Mater. Res.* **1988**, *3*, 787−797.
(45) Ishigame, M.; Sakurai, T. *J. Am. Ceram. Soc.* **1977**, *60*, 367−369.
(46) Kumar, S.; Bhunia, S.; Ojha, A. K. *Phys. E (Amsterdam, Neth.)* **2015**, *66*, 74−80.
(47) Feinberg, A.; Perry, C. H. *J. Phys. Chem. Solids* **1981**, *42*, 513−518.
(48) Ghosh, A.; Suri, A.; Pandey, M.; Thomas, S.; Ramamohan, T.; Rao, B. *Mater. Lett.* **2006**, *60*, 1170−1173.
(49) Hertl, W. *Langmuir* **1989**, *5*, 96−100.
(50) Jung, K. T.; Bell, A. T. *J. Mol. Catal. A* **2000**, *163*, 27−42.
(51) Mamivand, M.; Zaeem, M. A.; El Kadiri, H.; Chen, L. *Acta Mater.* **2013**, *61*, 5223−5235.
(52) Zhu, W. Z.; Lei, T. C.; Zhou, Y.; Ding, Z. S. *Mater. Chem. Phys.* **1996**, *44*, 67−73.

(53) Zhu, W. Z.; Lei, T. C.; Zhou, Y. *J. Mater. Sci.* **1993**, *28*, 6479−6485.
(54) Bolis, V.; Cerrato, G.; Magnacca, G.; Morterra, C. *Thermochim. Acta* **1998**, *312*, 63−77.